International Journal of Technology (2016) 2: 296-305
ISSN 2086-9614

CHARACTERISTICS OF VORTEX RING FORMATION BY SYNTHETIC JET ACTUATORS IN DIFFERENT CAVITIES

Engkos A. Kosasih[1], Harinaldi[1], Ramon Trisno[2*]

[1]*Departement of Mechanical Engineering, Faculty of Engineering, Universitas Indonesia, Kampus UI Depok, Depok 16424, Indonesia*
[2]*Departement of Mechanical Engineering, faculty of Engineering, University of Pancasila, Jagakarsa, Jakarta 12640, Indonesia*

(Received: October 2015 / Revised: December 2015 / Accepted: January 2016)

ABSTRACT

This paper presents a baseline study of the development of turbulent flow separation for controlling aerodynamic phenomena, especially in the design of the vehicle body. The purpose of this study was to analyze the performance of synthetic jet actuators (SJAs) as one of the tools that can be used in reducing the flow controller separation area on the bluff body model of the vehicle. To get maximum results in the performance of the SJA, this research starts with characterizing the actuator, including changes in the shape of the cavity and orifice diameter. Cavity shapes tested were half-ball (B), tube (T) and cone (K), while orifice diameters of 3, 5 and 8 mm were examined. The study was conducted using both computational and experimental approaches. Results from both types of research methods were compared and displayed in graphical form. These results serve as a reference for determining future research. The experimental results, in the form of the flow rate for each type of cavity, determined the ability of different cavity conditions to form vortex rings, whereas in CFD simulations, the formation of vortex rings was demonstrated via the visualization of flow contours. Vortex rings occurred in cavity conditions B3, T3, T5, K3 and K5. Vortex rings were not formed on any type of cavity with an orifice having a diameter of 8 mm.

Keywords: Bluff body; Reverse Ahmed body; Synthetic jet actuator; Vortex ring

1. INTRODUCTION

Global warming has been one of the main problems facing the world in recent years. The International Energy Agency, in its 2007 world energy outlook report, concluded that emissions of greenhouse gases will increase 57% by 2030 (IEA, 2007). In 2001, the Intergovernmental Panel on Climate Change (IPCC) determined that human activity was the primary cause of the greenhouse effect and the increase in global temperature in the 20th century (GIEC, 2001). One of the human activities that cause these problems are in the field of transport. Significant increase in the number of vehicles will be in line with the increase in fuel consumption and will cause environmental pollution and air pollution.

Due to these circumstances, the latest research in the field of vehicle aerodynamics has been carried out from the design standpoint of efficiency and with the goal of finding ways to positively impact fuel economy. For this reason, ground vehicle aerodynamics have been studied experimentally and numerically by many researchers.

*Corresponding author's email: ramontrisno@gmail.com, Tel. +62-21- 7864730 Ext.101, Fax. +62-21- 7270128
Permalink/DOI: http://dx.doi.org/10.14716/ijtech.v7i2.2986

Most previous studies have used simple models of vehicles that can generate the relevant features of air flow around a real vehicle (Ahmed et al., 1984; Hintenberger et al., 2004; Fares, 2006; Minguez et al., 2008; Uruba et al., 2009; Conan et al., 2011). The flow field around the wake is marked by a pair of horseshoe vortices and trailing vortices emanating from the edge of the sloping sides of the body (Ahmed et al., 1984).

There have been many experiments on passive flow control in wind tunnel model or prototype vehicles (Gad-el-Hak, 1996; Hucho et al., 1993). However, passive flow control in fact produces a weak effect in the vehicles involved because the nature of the air flow is turbulent and the contribution of friction on aerodynamic barriers is still small, only about 10% (Kourta et al., 2009).

One of the main issues in aerodynamics research is developing methods of flow control on the bluff body in order to reduce drag and noise (Hucho, 2002). The difference in pressure between the front and the back of the bluff body is a major contributor to the overall drag; the difference is primarily due to flow separation at the rear of the body (Hucho, 2002).

The need for a reduction in the drag force effectively encourages automotive designers to be more creative in developing innovative active control models. Active control models make it possible to modify the topology of the flow without changing the shape of the vehicle. Within the scope of academic and industrial laboratories, active control methods have been and are still being developed using both computational and experimental methods, and significant results have been obtained in the academic framework (Gad-el-Hak, 1996).

Flow active control in the form of a continuous blowing of placed on the back of a generic square back bluff body gives a drag reduction of 20% (Rouméas et al., 2009a). The same was done by Bruneau et al. (2011), in which the active flow control used was a combination of three were placed on the back of Ahmed body models, which resulted in drag reduction of 13%. A numerical study conducted by Rouméas et al. (2009b). Rouméas et al. (2009b) used active control of a synthetic jet that was placed on top of the rear window of an Ahmed body model, and drag reduction of 13% was obtained.

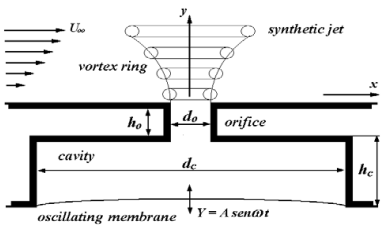

Figure 1 Diagram of a synthetic jet formed by an actuator in a cavity with an outlet orifice

Recently, developments in the active control of synthetic jets have mostly resulted from research conducted on the use of active control in the field of synthetic jet cooling and characterization of active control. Fluid jets in the form of air or other liquids have been used for the cooling of electronic equipment on a small scale. While synthetic jets have also been applied on Ahmed bodies to study the performance of the synthetic jet drag reduction, this research has not been carried out in depth; thus far it has only been demonstrated that the installation of synthetic jets can reduce aerodynamic drag on the vehicle (Harinaldi et al., 2011).

The application of synthetic jets mounted on a condition of a reverse Ahmed body has never been done in previous research. Reversing the Ahmed body is done to change the orientation of the flow direction before it is installed on the Ahmed body. This model describes the shape of the vehicle as often used in Indonesia. The synthetic jet will be installed on the top of the curve

of the Ahmed body. Before the synthetic jet is mounted on a vehicle it is necessary to research the characteristics of the synthetic jet, especially in terms of its influence frequency on the performance of the SJA due to changes in the shape of its cavity and orifice diameter. The purpose of this study was to determine the characteristics of the SJA by varying the shape of the cavity and the size of the orifice diameter and varying the frequency of oscillation to the membrane in order to induce a variety of vortex rings with such changes.

2. EXPERIMENTAL SETUP

Before studying synthetic jet performance on the reduction of drag on a vehicle, it is important to know about the performance of the SJA itself, in order to understand how to get the maximum results for drag reduction.

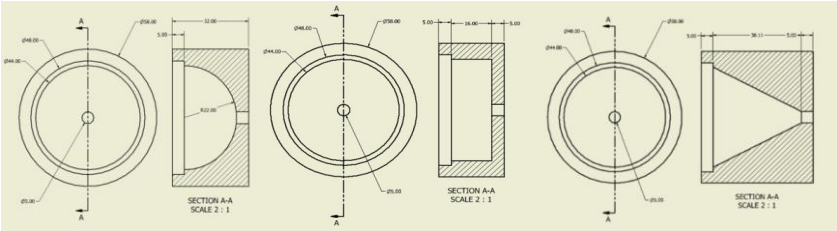

Figure 2 Possible shapes of the cavity: half ball (B3, B5, B8), tube (T3, T5, T8) and cone (K3, K5, K8)

Selection cavity is based on the SJA's cavity shape and orifice diameter and comparisons of their performances through experiments and CFD simulations. In this study, the SJA cavity shapes were a type of half ball, tube and cone; three versions of each shape were used, with diameters of 3, 5 and 8 mm (Figure 2).

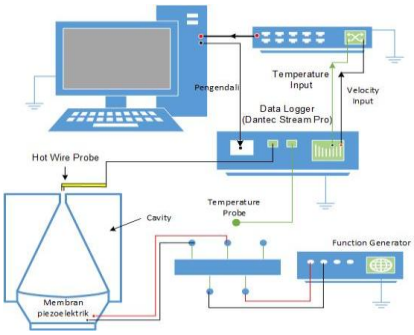

Figure 3 Schematic of the method for testing the performance of the synthetic jet

Figure 4 Piezo electric membrane

Figure 3 is a schematic diagram of the method of testing the synthetic jet's performance through experimentation. The testing platform consisted of a synthetic jet cavity and piezo electric membrane components, installed as a whole and driven by means of the function generator. This tool unleashed a wave of the desired signal. In this experiment the signal used is a sinusoidal wave. Movement of air was what caused the membrane to be pushed out of the cavity and pulled back into it. Piezo electric had a mechanical system with a very small mass of the stem and the spring move (Figure 4). This mass was suspended just two microns (two millionths of a meter) from the electronic circuit.

The velocity of the air that came out of this cavity through the orifice was measured using a hot wire probe (type 55P14 Gold Plate). This probe consisted of a manifold single wire with a diameter d_w = 5μm and a branch distance of 1.2 mm, placed as close as possible to the SJA; in

this case the possible distance was equal to ± 0.5 mm above the SJA's orifice, so that movement of the probe along the axis x did not contact or cause friction with the cavity.

The wire probe was connected to the data logger module (Dantec CTA Stream Pro type 91C10) that recorded the incoming data in the form of low voltage. Then the data was entered into the data acquisition board (National Instruments BNC-2110). This tool was used to convert analog data into digital data. The tool was connected to the computer via a data cable. The computer was also connected to a data logger that served to control the speed of recording the desired data at the time of data capture. The probe first had to be calibrated using a calibration unit (Dantec Streamline Pro Automatic Calibrator System S/N 9091H0013445), and King's Law was suitable for interpreting the data speeds below the calibration range. The range of the calibration was performed at 0.02 to 30 m/s before each experiment was done.

The uncertainty of the calculation results due to calibration for all data retrieval velocities is about 2.5%. The profile across the radial velocity measured with the hot wire probe using the tool transfer (vise) by the displacement distance was measured using a dial indicator with 0.01 mm accuracy.

The velocity data retrieval procedure was done under two conditions. First was a procedure to identify the frequency that produces the maximum velocity. The process of data collection was intended to determine the maximum velocity that can be generated by the SJA and the amount of data allowed (uncertainty) by varying the frequency of the sinusoidal wave issued by the function generator. The given frequencies ranged from 20 to 200 Hz. As many as 60,000 data points at a data velocity of 30,000 data / s were collected. The second procedure was measuring the jet velocity at points determined by the fishing coordinates (*X/D, Y/D*). Jet velocity was measured only in half of the region, because the jet is considered symmetrical while it is occurring. The values of *X/D* were 0, 0.25, 0.5, 0.75, ... 4, while the values of *Y/D* were 0, 1, 2, 3, ... 10. Speed data was recorded at 10,000 data points/s for 6 seconds.

This stage of research utilized computational simulations using CFD from ANSYS software. The purpose of these simulations was to get an initial overview of the performance of the SJAs to be studied and gather the CFD simulation results to be compared with the results of experiments as well as to visualize the vortex ring that happens to SJAs.

The criteria used in the experiment equated with the criteria used in this CFD simulation. However, the determination of the frequency used in CFD simulations was based on experimental results that were achieved, such as the use of User Defined Function (UDF) in the simulation that matched the experimental results.

3. RESULTS AND DISCUSSION

3.1. Testing Frequency and Mesh Independencies

The early stages of the experiment were to determine the frequency that produces the maximum flow rate that the SJA's can perform to use as a reference in subsequent experiments. This testing was done by varying the frequency of the sinusoidal wave created by the wave function generator tool.

Figure 5 shows graphics for the performance testing of SJAs performed using different frequencies with each cavity and the size of the orifice diameter. The maximum frequency of SJAs was selected based on the velocity at which the air flow out of the orifice reached maximum conditions. The maximum jet velocity can be produced by each SJA at a frequency of 110–130 Hz, and the cavity with a conical shape and orifice diameter of 3 mm produces the maximum jet velocity, at an average of 9.9249 m/s.

The frequency test was then used as a reference frequency in the simulation method. The maximum frequency was used in the UDF. The results of this simulation aimed to establish the type of meshing to be used to obtain simulation results closer to the experimental results.

In the computational method conducted by means of CFD simulations, meshing manufacture was done using Gambit software, while meshing testing was performed using Fluent software (6.3.26). This meshing testing aimed to get meshing that could produce CFD simulation results closer to the calculation results of experiments that have already been done. The meshing tested consisted of three forms, namely coarse, intermediate and fine, as shown in Figure 6.

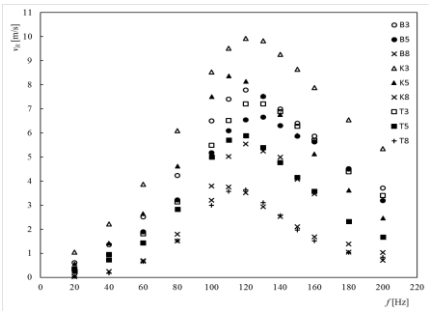

Figure 5 Graph of test results on some of the SJA cavities with sinusoidal signal types

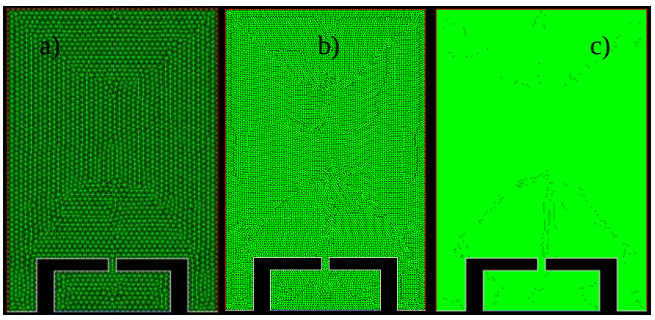

Figure 6 Meshing on the cavity shape of a tube with orifice diameter of 3 mm (T3): (a) Coarse; (b) Intermediate; (c) Fine

Each of these forms of meshing is then processed using Fluent software. The results of the different iterations created with this software can be seen in Figure 7, which shows a comparison of the measurement results obtained through experiments compared with the results of the various CFD simulation iterations. From this figure it can also be seen that there was harmony between the experimental results and CFD simulations on the velocity of the jet at the SJA-specified intervals.

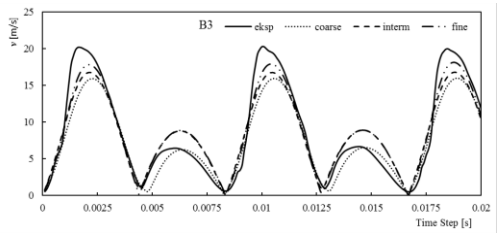

Figure 7 (a) Graph jet velocity comparison of meshing test results in CFD simulations and experiments in B3

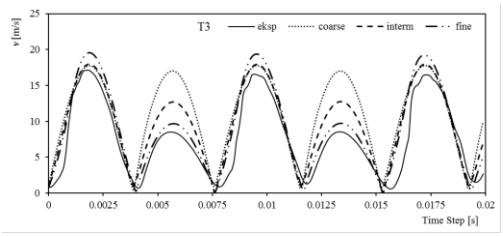

Figure 7 (b) Graph jet velocity comparison of meshing test results in CFD simulations and experiments in T3

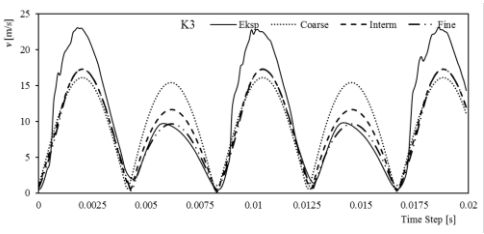

Figure 7(c) Graph jet velocity comparison of meshing test results in CFD simulations and experiments in K3

The CFD simulations and experimental results illustrate the results of the jet velocity at the position *X/D* = 0 and *Y/D* = 0 with the speed of the data recording at 10.000 data points persecond. The determination of frequencies that can provide maximum jet velocity and the results of each iteration for meshing in CFD simulations can be seen in Table 1.

Table 1 The maximum frequencies of jet velocity and type of meshing in CFD simulations and experiments

No	Cavity type	Experimental	CFD Simulation
1	B3	120 Hz	Fine
2	B5	130 Hz	Fine
3	B8	120 Hz	Coarse
4	K3	120 Hz	Fine
5	K5	110 Hz	Coarse
6	K8	110 Hz	Fine
7	T3	130 Hz	Fine
8	T5	120 Hz	Fine
9	T8	120 Hz	Intermediate

3.2. Uncertainty in Experimental Methods and Simulation CFD

The measurement results are the estimated value of the quantity being measured. Uncertainty of quantitative measurements is not reported as a single value but is reported with a range of values. Measurement results vary reflecting the deviation caused by performance factors of tools, methods of measurement, environmental conditions, and so forth.

Uncertainty aims to determine the extent of validity in gathering the amount of data. Data recording in this experiment was carried out as many as 60,000 times per 6 seconds (10,000 data points/s). The simulation data was also recorded as many as 10,000 times per one second, with a 95% confidence level. So:

$$U_x \propto \sigma_{\bar{x}} \Rightarrow U_x \approx k(\text{convidence limit})\,\sigma_{\bar{x}} \tag{1}$$

Graphing the results of the calculation of uncertainty for each cavity shape was done based on the number of data points recorded per second, which was 10,000 in this case. The processed data was data that occurred on the condition *Y/D* = 0 and *X/D* = 0. The point (0,0) was 0.5 mm above the orifice hole, so that the movement of the probe was not in contact with the surface of the SJA.

Figure 8 charts the results of calculations of data uncertainty based on the equations that exist in each type of cavity.

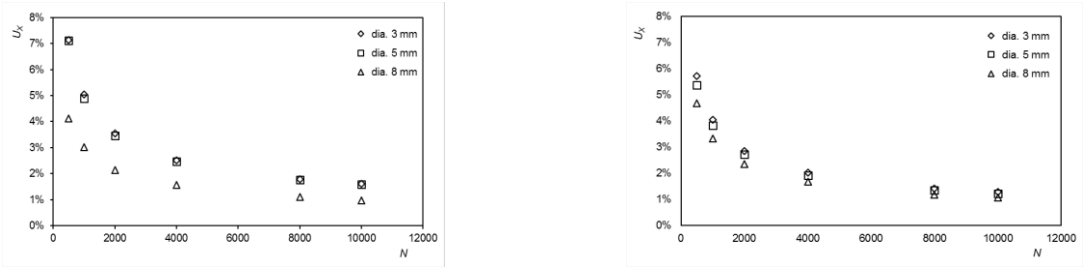

(a) (b)

Figure 8 Graph uncertainty for flow velocity in the cavity with a half-ball shape: (a) experiment; (b) CFD simulation

Based on data obtained from experiments and CFD simulations, the B3 value had greater uncertainty compared to other cavity types and orifice sizes. Uncertainty in the experimental methods was 1.6081% and the value of CFD simulation results amounted to 1.2789%. While the value of the smallest uncertainty occurred at B8, uncertainty of its value was 0.98% for the experimental methods and 1.0632% for the CFD simulation method. The value of this uncertainty needs to be considered with regard to magnitude, so that the amount of data captured in the experimental conditions and CFD simulations can meet a confidence level of 95%, and the uncertainty of its value must be below 5%. In both these methods, this has been fulfilled.

3.3. Determining the Vortex Ring

Characteristics of the flow velocity at the SJA were taken from the velocity at the center line, U_{CL}, as the assumption was that the highest velocity profile was at the exit orifice. The spatial velocity profile can show the standard deviation of the highest form, and some of the speed scale was time for the average flow rate through the expulsion stroke, namely:

$$U = \frac{1}{T/2}\frac{1}{A_n}\int_{A_n}\int_0^{T/2} U(t, A_n)dtdA_n \tag{2}$$

Where U was velocity of the average axial phase, T was the period of excitation and A_n was the cross-sectional area of the exit orifice. The average velocity can be used to determine the jet's Reynolds number. The important thing at the length scale of the synthetic jet stream was the stroke length, L_o/D, namely:

$$L_o = \int_0^{T/2} U_{ave}(t)dt \tag{3}$$

Spatially, U_{ave} was an average flow velocity. Stroke length was the distance the fluid traveled during the process of pushing the fluid from the cavity.

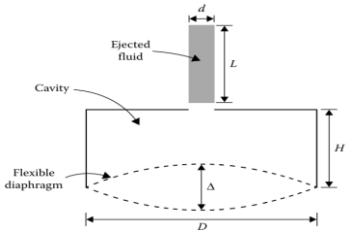

Figure 9 Stroke length on a synthetic jet

Excitation frequency can be non-dimensional as numbers of strokes, S, namely:

$$S = \sqrt{\frac{2\pi f D^2}{\nu}} \tag{4}$$

The non-dimensional parameter uniquely determined the operating conditions of the SJA and so affected its ability to transfer linear momentum. In particular, Holman et al. (2005) showed that in order to reach the exit after an expulsion stroke, a vortex is defined as synthetic jet formation, in which:

$$\frac{\mathrm{Re}_U}{S^2} > C \tag{5}$$

where C is a constant equal to 0.16 for the symmetric axis and 1 for rectangular nozzles. According to Holman et al. (2005), the condition of the occurrence of a vortex ring was $Re_U/S^2 > 1$. Meanwhile, Smith and Swift (2001) found the ring vortex can occur if:

$$\frac{L_0}{D} = St > 6 \tag{6}$$

Table 2 The results of calculations of the occurrence of vortex rings on the experimental method

Cavity	Re_U	Re_U/S^2	L_o/D
B3	1201.32	2.768	16.248
B5	1092.08	0.836	5.25
B8	1367.35	0.443	2.782
T3	1837.03	3.92	12.31
T5	2469.24	2.055	6.453
T8	2464.2	0.801	2.516
K3	1418.34	3.05	19.20
K5	1711.13	1.44	9.09
K8	1091.83	0.36	2.26

In addition to the calculation of the equation by incorporating existing experimental results, the ring vortex can also be proved by means of CFD simulations. The simulation results also were matched with the results of the calculations that had been done previously. The results of this simulation can be seen in Figures 10a to 10c below.

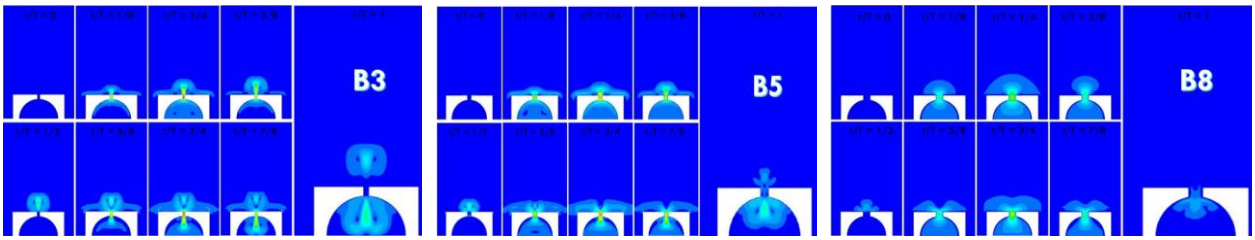

(a) (b) (c)

Figure 10 The formation process of vortex rings in condition: (a) B3; (b) B5; and (c) B8

Figures 10a to 10c show the process of the formation of a vortex ring cavity with a half-ball shape and orifices with diameters of 3, 5 and 8 mm respectively using FLUENT software. Figure 10a shows the contour of flow velocities caused by the movement of the membrane in condition B3. If the membrane moves and is at t/T = 1/8, then in this position the membrane is pushing, hence the visible presence of air flowing out through the orifice.

Then at position t/T = 1/4, the contour of flow velocities was beginning to show the formation of vortex rings. Position t/T = 1/4 is the peak of the expulsion stroke undertaken by the movement of the membrane. The membrane began to move down or the SJA began to suction, and after reaching position t/T = 3/8 the vortex ring could be seen more clearly. After reaching position t/T = 1/2, this vortex ring section started to break away and moved further away from the end of the orifice. The suction movement continued to position t/T = 5/8; in this position the

air under the vortex ring was partly drawn back into the cavity. This affected the shape of the ring vortex which was formed by blowing. The vortex ring that had been formed remained intact and further intensified in position t/T = 3/4. Then in position t/T = 7/8, the membrane moved up, and the SJA started blowing. In this position the vortex ring had been formed and was ready to break away because of the formation of a new vortex ring. At position t/T = 1, the vortex ring had released themselves from the end of orifice.

Figure 10b shows the contours of a velocity jet produced by SJA condition B5. In these pictures, it is clear that a ring vortex began to form at position t/T = 1/4. Then in position t/T = 3/5, ring vortices began to move to separate from the end of the orifice. It is more noticeable in position t/T = 1/2 that the ring vortex left the end of orifice. But when the membrane moved down at position t/T = 5/8, the cavity began doing suction, so that most of the air around the orifice began to be drawn back into the cavity, and the ring vortex that had been formed was plagued by suction, as shown in position t/T = 3/4. Consequently, vortex rings broke out again at position t/T = 7/8 and vortex rings failed to form, as shown in position t/T = 1.

Figure 10c shows the contours of the velocity jet produced by SJA condition B8. At the beginning of blowing conditions, the speed contours form a ring vortex. So also when the suction, which is at position t/T = 5/8, began, most of the air at the end of the orifice can be seen flowing back into the cavity and filling the interior of the cavity. This situation makes the vortex ring formed by SJA condition B8 invisible. Thus, it can be said that the experimental method and CFD simulation methods gave the same result.

4. CONCLUSION

From the results of this research on the characteristics of SJAs, some conclusions can be reached. The maximum speed that can be generated by an SJA is in the frequency range 110–130 Hz with an uncertainty of 2% to the amount of 10,000 data points per second. The most high-velocity jet was produced by the K3-type cavity, which had a conical shape and an orifice with a diameter of 3 mm. The average jet velocity reached 9.98 m/s. The vortex ring can be determined by both experimental and CFD-simulation methods, as both of these methods give the same result. In addition to the experimental method described in this paper, other researchers (Glezer, 1988; Smith et al., 2001) have demonstrated that issuing the equation of the formation of a vortex ring has the same result. A vortex ring can occur in conditions B3, T3, T5, K3 and K5. A vortex ring was not formed on any shape of cavity with an 8-mm-diameter orifice.

5. REFERENCES

Ahmed S.R., Ramm G., Faltin G., 1984. Some Salient Features of the Time-averaged Ground Vehicle Wake. *SAE Technical Paper 840300*

Bruneau, C.-H., Creusé, E., Depeyras, D., Gilliéron, P., Mortazavi, I., 2011. Active Procedures to Control the Flow Past the Ahmed Body with a 25° Rear Window. *International Journal of Aerodynamics*, Volume 1(3/4), pp. 299–317

Conan, B., Anthoine, J., Planquart, P., 2011. Experimental Aerodynamic Study of a Car-type Bluff Body. *Experiments in Fluids*, Volume 50(5), pp. 1273–1284

Fares, E., 2006. Unsteady Flow Simulation of the Ahmed Reference Body using a Lattice Boltzmann Approach. *Computers & Fluids*, Volume 35(8–9), pp. 940–950

Gad-el-Hak, M., 1996. Modern Development in Flow Control. *Applied Mechanics Review*, Volume 49(7), pp. 365–379

Glezer, A., 1988. The Formation of Vortex Rings. *Physics of Fluids*, Volume 31(12), pp. 3532–3542

Groupe d'experts Intergouvernemental sur l'Evolution du Climat (GIEC), 2001. *Bilan 2001 Des Changements Climatiques: Les Éléments Scientifiques*. Available online at: http://www.developpement-durable.gouv.fr/Rapports-d-evaluation.html, Accessed on 27 January 2015

Harinaldi, Budiarso, Tarakka R., Simanungkalit S.P., 2011. *International Journal of Mechanical & Mechatronics Engineering IJMME-IJENS,* Volume 11(03), pp. 24–30

Hintenberger, C., Garcia-Villalba, M., Rodi, W., 2004. *The Aerodynamics of Heavy Vehicles: Trucks, Buses, and Trains*. Berlin: Springer

Holman, R., Utturkar, Y., Mittal, R., Smith, B.L., Cattafesta, L., 2005. Formation Criterion for Synthetic Jets. *AIAA Journal*, Volume 43(10), pp. 2110–2116

Hucho, W.-H., 2002. *Aerodynamik der stumpfen Körper-Physikalische Grundlagen und Anwendung in der Praxis*. Braunschweig: Vieweg-Verlag

Hucho, W.-H., Sorvan, G., 1993. Aerodynamics of Road Vehicles. *Annual Review of Fluid Mechanics*, Volume 25, pp 485–537

International Energy Agency (IEA), 2007. *World Energy Outlook, China and India Insights*. Paris: OECD/IEA

Kourta, A., Gilléron, P., 2009. Impact of the Automotive Aerodynamic Control on the Economic Issues. *Journal of Applied Fluid Mechanics*, Volume 2(2), pp. 69–75

Minguez, M., Pasquetti, R., Serre E., 2008. High-order Large Eddy Simulation of Flow over the "Ahmed Body" Car Model. *Physics of Fluids*, Volume 20(9), pp. 095101-1–095101-1

Rouméas, M., Gilléron, P., Kourta, A., 2009a. Analysis and Control of Near-Wake Flow over a Square-back Geometry. *Computers & Fluids*, Volume 38(1), pp. 60–70

Rouméas, M., Gilléron, P., Kuorta, A., 2009b. Drag Reduction by Flow Separation Control on a Car after Body. *International Journal for Numerical Method in Fluids*, Volume 60(11), pp. 1222–1240

Smith, B.L., Glezer, A., 1998. The Formation and Evolution of Synthetic Jets. *Physics of Fluids*, Volume 10(9), pp. 2281–2297

Smith, B.L., Swift, G., 2001. *Synthetic Jets at Large Reynolds Number and Comparison to Continuous Jets.* Postdoctoral Research. USA: American Institute of Aeronautics and Astronautics

Uruba V., Hladik O., 2009. On the Ahmed Body Wake. In: *Conference Colloquium FLUID DYNAMICS*, Prague

Utturkar, Y., 2002. *Numerical Investigation of Synthetic Jet Flow Fields*. M.S. Thesis, Department of Mechanical Engineering, University of Florida